

A Force Sensor for the Control of a Human-like Tendon Driven Neck

M. Fumagalli, L. Jamone, G. Metta, L. Natale, F. Nori, A. Parmiggiani, M. Randazzo, G. Sandini

Italian Institute of Technology

Via Morego 30, Genova, ITALY

{matteo.fumagalli,lorenzo.jamone,giorgio.metta,lorenzo.natale,francesco.nori,alberto.parmiggiani,marco.randazzo,giulio.sandini}@iit.it

Abstract—This paper describes the design and realization of a force sensor and its use in the control of a human-like robotic neck actuated with tendons. The sensor is designed to have high sensitivity and to be robust to large loads. We use the sensor to control the force exerted by the tendons and realize a controller for the two degrees of freedom of the neck. With respect to previous work [1] we show that the use of force feedback improve the robustness of the controller. Although quite specific to the robotic setup that we considered the work we describe shows some insights that could be useful for the control and realization of similar structures actuated with tendons.

I. INTRODUCTION

The past years have seen humanoid robots becoming more dexterous and compact with several attempts to realize actuation structures that closely resemble those of humans. Somewhat extreme examples in this direction are represented by the robots Cronos [2] and Kotaro [3]. More traditional actuation systems are instead used in humanoid robots like the iCub and ARMAR-III [4], [5]. One of the challenges in the design of such robots is the placement of the actuators. To reduce size, weight and inertia of the mechanical structure of the robots it is often preferable to place the motors in proximal joints and route the actuation to distal ones. Tendons are widely adopted for this purpose, since they allow sophisticated routing of the actuation but still guarantee a light weight solution and low friction. The control of tendon-driven joints is however difficult. To operate correctly the tension of the tendons must be maintained within certain limits. This avoids breakages (in case of too large stress) or that the tendon becomes slack and hence difficult or impossible to control. Besides, tendon driven joints are often overactuated (e.g. agonist-antagonist configuration) and pose additional challenges from a control point of view.

Safety is another issue attracting the attention of researchers in the field. To reduce the risks of damages or injury due to unexpected interaction with the environment, a common choice is to limit the amount of force exerted by the robot by either controlling the torque produced by the motors or by reducing the mechanical impedance of the links. Although the advantages of torque control are well known in the literature [6], [7] the latter is rarely implemented in humanoid robots. This is mainly due to technological limits. Commercial force sensors are usually expensive and rarely fit in the space available on the joints or links of robots.

In this paper we describe the realization of a force sensor for the control of the neck of a humanoid robot. The neck consists in a spring that is actuated by three surrounding tendons. Motion is controlled by pulling the motors with three electric motors. A possible control schema for this neck has been already proposed in [1]. In this paper we show that force feedback simplifies the controller and improves the robustness of the system. Although the problem we address seems very specific to the robotic setup we used, the work we describe can give some insights that can be applied to the control of similar structures.

The remainder of the paper is organized as follows. In Section II we give a detailed description of the robotic setup. In this section we describe the mechanical structure of the neck and formulate the control problem. In Section III we describe the design of the force sensor and its validation using Finite Element Analysis. In Section IV we describe the control of the neck using different approaches, with and without force control. In Section V we compare the performance of the different approaches in terms of robustness. Finally Section VI, we draw the conclusions.

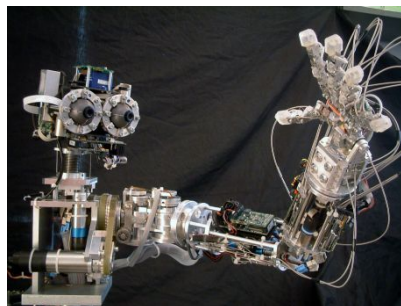


Fig. 1. The humanoid robot James.

II. PLATFORM

The work described in this paper was carried out on James [8], a 22-DOF torso with moving eyes and neck, an arm and an anthropomorphic hand (see Figure ??). In the following subsections we provides details on the mechanical structure of the neck and its actuation system.

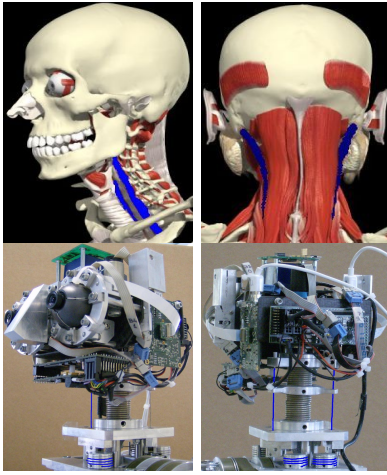


Fig. 2. Top. Human neck muscles we took inspiration from in the system design, highlighted in blue: *Longus Colli* in the left image, and *Longissimus Capitis* in the right image (images taken from *Primal 3D Anatomy* software [12]). Bottom. James neck tendons are arranged like the human muscles highlighted in the top images.

A. The neck design

The neck “bone” consists in a steel spring, which supports the head while providing it the possibility to bending forward and laterally (respectively pitch and roll) (see Figure 3). The actual pitch and roll positions are measured through an inertial sensor placed on the top of the head. The actuation of the two degrees of freedom is obtained with a structure that recalls the design of a tendon-driven parallel manipulator (recent studies on this kind of actuation, in [9], [10]). Three steel tendons surround the neck and exert force in three points placed 120 deg apart on the top of the neck (the top “vertebra”). These forces bend the spring and, therefore, produce the movement of the neck along the pitch and roll dimensions. Tendons are routed along the spring through capstans placed on a second “vertebra”. The length of the tendons is adjusted by three motors, positioned at the base of the neck (see Figure 3).

This special geometry allows the neck to have ranges of motion comparable to a human; as claimed by Clarkson [11], average ranges of motion for pitch and roll rotations in adults are about ± 45 deg, while James motion is in the range of ± 40 deg (the mechanical limits are actually wider, but they are here been limited for safety reasons).

Even if far from being a close reproduction of the human musculoskeletal system, this structure has some analogies with the arrangement of some of the human neck muscles (see Figure 2). Humans are provided with more than 20 types of muscles in the neck, with several units for each type, settled into different layers: their work is both to control the orientation of the head with respect to the neck base and to give stability to the cervical spine in supporting the weight of the head [12]. In our system, the spring tone is sufficient to support the head, and the tendons are employed just to move the head along the roll and pitch axes. More information about the neck can be found here [1].

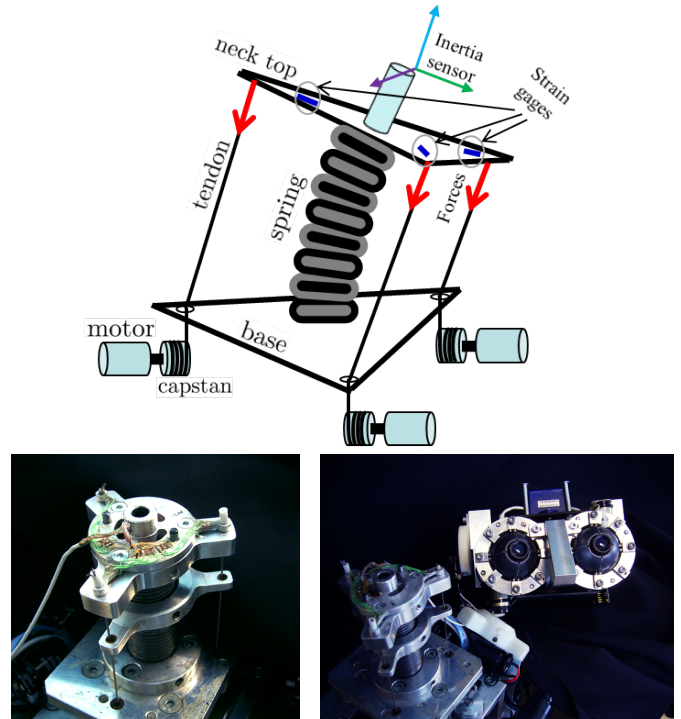


Fig. 3. Sketch of the neck actuation system and kinematics (Top). Each motor pulls a tendon which passes through a hole in the neck base. In this way the effective tendon length can be reduced to bend the spring in different directions. On the bottom, views of the neck sensor from the top (left) and of the disassembled platform (right)

B. Redundancy of the actuation scheme

A tendon-driven system with open-ended tendons (i.e. tendons that can exert tension but not compression) requires more tendons than DOFs to be fully controllable. Therefore, to independently control n DOFs, $n + 1$ tendons (and motors pulling the tendons) are needed [13]. In our setup, the position of the end effector is a two dimensional variable, $x \in \mathbb{R}^2$, corresponding to the head pitch and roll. This variable is controlled by the position of the three motors, $q \in \mathbb{R}^3$. Remarkably, given the head configuration, there are mechanical (and practical) constraints which prevent the motor positions q from being chosen arbitrarily. In practice, for a given head posture x there is an ideal motor configuration q^* which distributes the stresses over all the three tendons in an optimal way. Given the elasticity of the structure, the actual motor configuration q can differ from q^* but the more the distance $q - q^*$ the higher the risks of compromising the actuation structure (see also [1]). High tendon tension might break the tendon and low tension might misalign the tendon with respect to its capstan.

To better understand the structure of the problem, let us consider the simple case of a 2D device, where we have two independent motors to actuate a single degree of freedom (nominally the slope of the surface on which the head is mounted). In the assumption that the spring is compressed (so that it can only bend), this system is redundant (see Figure

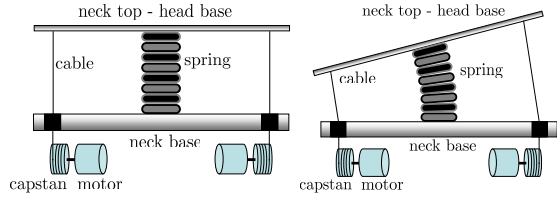


Fig. 4. Equivalent two dimensional scheme of James's neck.

4). For example, shortening both cables of the same length does not produce any slope movement but it only increases the forces acting on the spring. This force (and the tension of the tendons) must be kept under control: large force will damage (misalign) the spring coils and low tensions cause the wrong alignment of the cables on the capstans. In this paper we handle this problem with the introduction of a sensing element that measures the force of each tendon. The design of the sensor is shown in III. Section IV instead presents two approaches for the position control of such redundant system. A comparison of the results achieved by these controllers is finally shown in section V. A comparison of the results achieved by these controllers are finally shown in section V.

III. THE FORCE SENSOR

The force sensors are positioned on the upper “vertebra” of the neck (see Figure 3). This solution was adopted because it was impossible to sense the force directly on the motors (due to the very limited empty space) or on the tendons. The latter solution was discarded because it would have excessively reduced the tendons range of motion. We connected each tendon to a cantilever beam that transmits the force applied by the motor to the top of the neck. A strain sensor placed on each cantilever beam senses the deflection produced by the force exerted by the motor. This design has many advantages: among all, it allows to easily add a mechanical stop which limits the deflection of each cantilever beam and protects the sensing elements (see Figure 5).

A. Design Specifications

The first requirement for the sensor was the capability to read loads in the range of $0 \div 100N$, which is the range of force the motors can produce.

Force is usually measured indirectly by sensing the deformation of a part that transmit the force: under the hypothesis of linear elasticity, force is directly proportional to the sensed deformation. To obtain high resolution and good signal to noise ratio it is preferable to design a structure which can generate the highest possible strain.

As mentioned, we used a cantilever beam structure (see Figure 5) in the neck joint. We estimate the tension of the tendon from the flexion of the beam structure. For this purpose we employed semiconductor strain gages (SSGs) in a Wheatstone bridge configuration. We preferred SSGs as opposed to more standard metal SGs, due to their higher sensitivity (less deformation is needed to produce the same effect), higher fatigue life and higher output signal.

A drawback of SSGs is their delicate attachment process¹. Since force is measured as a strain difference, placement errors in the gluing phase might introduce unwanted biases. Therefore, we designed the part in order to have constant strain in the region where the SSGs are glued: in this way an eventual placement error would not affect the measure of strains. One additional requirement for the sensor was robustness. A desirable characteristic for a force sensor is to withstand high impulsive loads (such as those caused by impacts). We solved this issue by restricting the maximum deformation of the sensing element with a mechanical limit thus posing a limit to maximum levels of stress that can occur in the structure (see Figure 5).

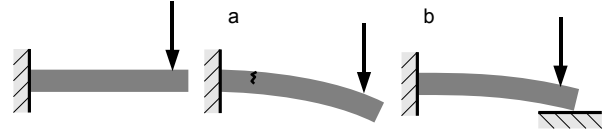


Fig. 5. Vertical deflection of a cantilever beam. A hardware limit at the beam end (b) can be used to limit the flexion that would otherwise cause failure (a).

B. Analytic Model

To obtain constant strain in the region where the SSG will be bonded we designed the beam to have a linearly growing cross-section: we then needed to determine the correct value for the parameters defining its shape (see Figure 6).

By employing the Euler-Bernoulli and linear elastic beam equations we determined the appropriate geometry of the deforming part, and its vertical displacement (see [14] for the detailed mathematical tractation).

¹In semiconductor strain gauges the change in resistivity depends on piezo-resistive effects of boron doped silicon. The semiconductor bonded SG is a thin slice of silicon substrate with the resistance element diffused into a substrate of silicon. The wafer element usually is not provided with a backing, and bonding it to the strained surface requires great care as only a thin layer of epoxy is used to attach it.

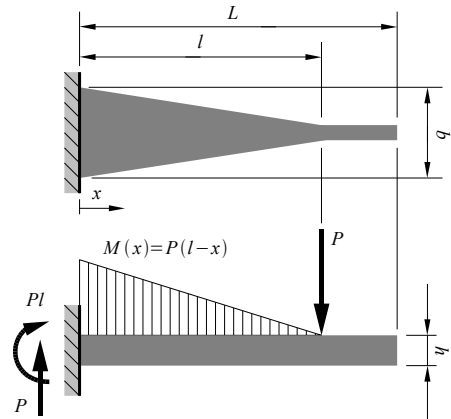


Fig. 6. Beam analytic model: geometric parameters definition. The cantilever has a growing section from the end-point to the base. The height is constant along the cantilever length. Using this shape, the strain is constant.

C. FEM Analyses

To validate the critical geometric parameter calculation we cross-checked the expected behavior of our sensor with a FEM analyses. We created a CAD model of our sensor, and then processed it with the Ansys Workbench Educational FEA software. Since the sensor is not affected by relevant non-linearities we chose to perform a linear elastic analysis. For its rather high mechanical resistance ($520MPa$ ca. tensile strength) we chose to use an aluminum-zinc-magnesium-copper alloy named Ergal7075. This material was then used for the production of the sensor.

The mesh was generated automatically with a patch independent tetrahedron algorithm with refinement conditions in the bending region to better model the stress/strain gradients (the meshed model is shown in Figure8).

For boundary conditions, $80N$ force, applied in the region where the tendon is fixed, was used to model the tractive load of the tendons.

To simulate the contact with the subjacent part the vertical displacements of the base of the sensor were constrained to be zero.

The stress field computed as a result of one of the analyses is shown in Figure 7. As it can be seen, the maximum Von Mises stress is $176.88MPa$, which is well under the maximum allowable stress (the safety factor can be estimated to be around 2.9).

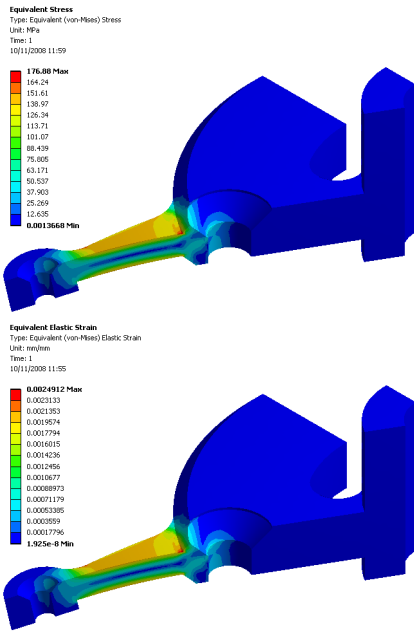


Fig. 7. Equivalent Von-Mises stress (Top) on the cantilever and equivalent strain (Bottom). The shape of the cantilever has been chosen such that the VM stress is constant on its length. The maximum strain on the cantilever should be less than the maximum strain of the SSG linear characteristic (in our case 2000μ -strain)

Figure10 shows a comparison of the theoretically and numerically calculated beam deflections. As can be seen the region where the prediction of the analytical model is less

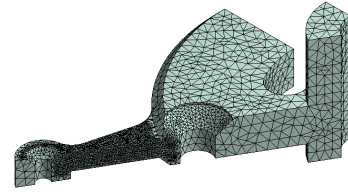


Fig. 8. Mesh generation for FEM analysis. The interesting part of the neck sensor (the cantilever) should be tickened with elements.

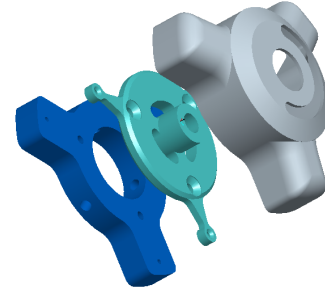


Fig. 9. Exploded view of the sensor. Starting from the left side the Figure show the base plate used as hard mechanical stop, the sensing element and the protection cover.

accurate is the end of the beam (de Saint Venants conditions are not fully met and there is a slight geometric discrepancy in the two models). Nevertheless the analytical solution nicely meets the result of the FEA in predicting the deformation of the region where the SSG will be attached. We therefore finalized the design and thickened the terminal part of the beam to correctly beat the hardware limit if needed: the final sketch of the sensor can be seen in Figure 9.

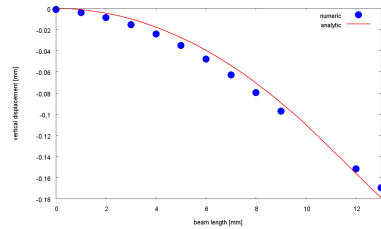


Fig. 10. Beam flexion: comparison of computed numerical and analytical vertical beam displacements.

IV. CONTROL

We would like to control the position of the three motors attached to the tendons, q so to steer the orientation of the neck, x ($[pitch, roll]^T$) to a desired value x_d ($[pitch_d, roll_d]^T$). In practice, the proposed controllers use a low level velocity control which allows us to directly control the individual motor velocities \dot{q} . Each controller computes the velocity command \dot{q} as a function of the positioning error $x - x_d$:

$$\dot{q} = f(x - x_d), \quad (IV.1)$$

while at the same time reducing the stress on the tendons to avoid brecking the structure (the spring or the tendons).

In this section we describe different controllers that approach this problem in different ways. In Section V we compare their performances.

A. Model based control

The model based controller exploits an inverse kinematic model of the system², $q^* = f_{inv}(x)$, and its Jacobian, J_{inv} , in order to reduce the position error to zero while keeping the tendons in a “good” configuration. The desired motor velocities, $\dot{q} \in \mathbb{R}^3$, are obtained as follows:

$$\begin{aligned} \dot{q} = & -J_{inv}(x)(x - x_d) + \\ & -(I - J_{inv}(x)J_{inv}^\dagger(x))(q - f_{inv}(x_d)), \end{aligned} \quad (IV.2)$$

where $q \in \mathbb{R}^3$ are the motor positions, $x, x_d \in \mathbb{R}^2$ are the actual and desired control variable configurations (pitch and roll rotations) and $I \in \mathbb{R}^{3 \times 3}$ is the identity matrix. The inverse kinematic model, $q^* = f_{inv}(x)$, defines a two-dimensional manifold in which motor positions q_d maintain the tendons with an ideal tension for a given x . This model somehow allows to regulate tendons tension even without any force measurement. The first part of the control law employs the Jacobian to cancel the inertial error, while the second part tries to keep the motor configuration as close as possible to the manifold (projecting in the Jacobian null-space). Further details can be found in [1].

B. Position Control with internal force feedback

In this subsection we describe a controller which explicitly uses force feedback. The controller is structured as follows: firstly, the position error $e_{pr} = x - x_d$ is converted into a fictitious instantaneous reference torque $\tau_d = [\tau_{pitch}, \tau_{roll}]^T \in \mathbb{R}^2$ according to following PID control:

$$\tau_d = k_p e_{pr} + k_d \frac{d}{dt} e_{pr} + k_i \int e_{pr} dt, \quad (IV.3)$$

where k_p , k_d and k_i represent the proportional, derivative and integral gain of the controller. Clearly, we do not have direct access to the torques applied at the pitch and roll degrees of freedom but a given τ_d can be realized by a suitable choice of the force $F_d \in \mathbb{R}^3$ applied at tendons. In particular, due to the system redundancy, the forces F_d that produce the desired τ_d are the ones in the following set:

$$\{F_d : \tau_d = J(\alpha, l)F_d\} = \mathcal{F}(\tau_d). \quad (IV.4)$$

Among all the possible vectors F_d in $\mathcal{F}(\tau_d)$, we want to pick one that has minimum norm but that also guarantees a minimum desired force f_{min} in all the components. This problem has been solved by choosing the vector F_d as the solution to the following optimization problem:

$$\min_{F_d \in (\tau_d)} \|F_d\| \quad s.t. \quad F_d \geq F_{min} \quad (IV.5)$$

where the operator \geq indicates that each component of vector F_d should be larger or equal to the corresponding component

²This model represents the ideal tendon configuration q^* given the head configuration x . See also Section II-B.

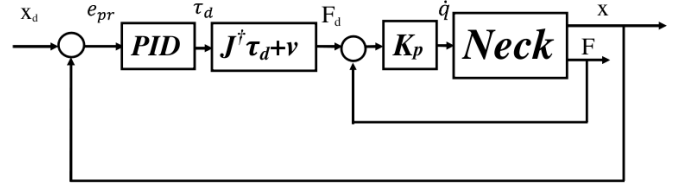


Fig. 11. Scheme of the neck controller. J^\dagger is the constant Jacobian matrix which transforms the equivalent torques imposed by the position controller into the reference tendon force to guarantee the motion.

of vector $F_{min} = [f_{min}, f_{min}, f_{min}]^T$, and $J(\alpha, l)$ is the transformation matrix projecting the tendon forces to the corresponding pitch and roll torques:

$$J(\alpha, l) = \begin{bmatrix} l & l \cos(\alpha) & l \cos(\alpha) \\ 0 & l \sin(\alpha) & -l \sin(\alpha) \end{bmatrix}. \quad (IV.6)$$

In the above formula, $l \in \mathbb{R}$ is the length of the cantilevers and $\alpha \in \mathbb{R}$ their relative angle. In our case the solution to this problem is (for more details see the Appendix):

$$\begin{cases} F_d = J^\dagger \tau_d + \lambda u \\ u = [1, 1, 1]^T \in \ker(J), \\ \lambda = F_{min} - \min(J^\dagger \tau_d) \end{cases} \quad (IV.7)$$

where $\min(\cdot)$ represents an operator that returns the smallest component of a vector and $F_d \in \mathbb{R}^3$ is the desired tendon force ($F_d = [F_{d1}, F_{d2}, F_{d3}]^T$). Finally, the desired forces F_d are realized by generating the velocities inputs \dot{q} according to the following proportional control law:

$$\dot{q} = K_f e_f, \quad (IV.8)$$

where $K_f \in \mathbb{R}^{3 \times 3}$ is the diagonal matrix of proportional gains and $e_f = F_d - F$ is the difference between the measured ($F \in \mathbb{R}^3$) and desired ($F_d \in \mathbb{R}^3$) forces. The stability of such system is not here analyzed, but the interested reader should refer to [6] and [7].

Finally, we want to limit the maximum desired force. At this aim we saturate F_d ; to guarantee good performance of the PID regulator we also introduced an anti-windup filter on integral component of the PID. A draft of the control scheme is reported in Figure 11.

V. RESULTS

In this section, we compare the control system of (IV-A) and the position control with internal force feedback of (IV-B).

Figures 12 and 13 show the step response of the two controllers (a_1 and b_1 , corresponding respectively to pitch and roll step response) showing measured x in red and x_d in blue. Desired positions are assigned every 15 seconds. The two controllers are similar in terms of step response. Figures a_2 and b_2 of Figures 12 and 13, instead, show the instantaneous error e_{pr} values at steady state, just before the new position command is imposed.

Figure 14 shows the response of the force controller to force commands (measured force F in red and desired force F_d

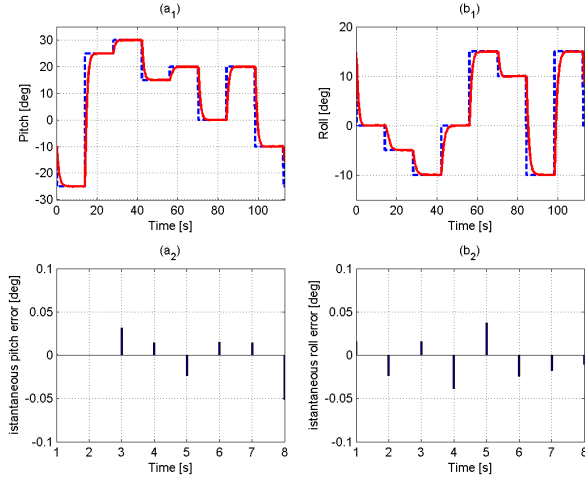


Fig. 12. Desired (blue dashed line) vs actual position (red line) using the position controller with Jacobian.

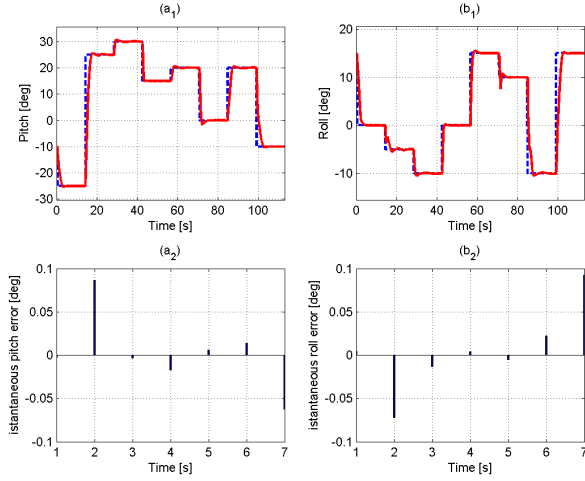


Fig. 13. Desired (blue dashed line) vs actual position (red line) using the position controller with inner force feedback (blue dashed line) along each tendon.

in blue). At steady state the controller always converges to the desired force (even though the force trajectories are not perfectly followed during transients, because of the coupling of the system).

Figures 15 and 16 compare the performance of the two controllers in terms of the force acting on the spring and tendons. Figure 15 reports the force exerted by each tendon during several movements. In absence of force feedback considerably larger loads are acting on the tendons. In some cases the lower limit of tension on the tendons is not met, causing possible tendon/capstan misalignment. When force feedback is used, on the other hand, forces are always within the desired range. Figure 16 reports the sum of the three forces which is (to a certain extent) related to the overall force acting on the neck spring. Overall these results prove that force

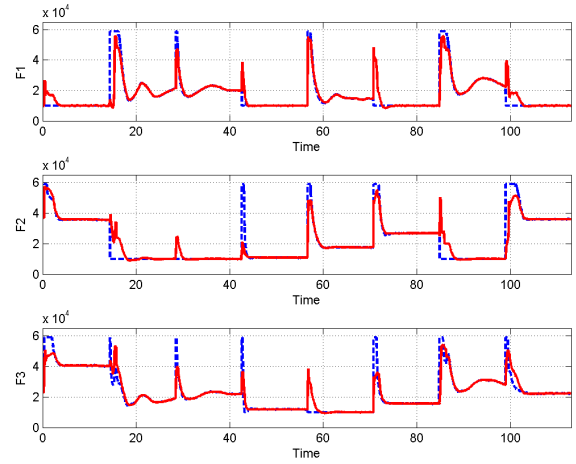


Fig. 14. Desired (blue dashed line) vs measured force (red line) using the position controller with inner force feedback along each tendon.

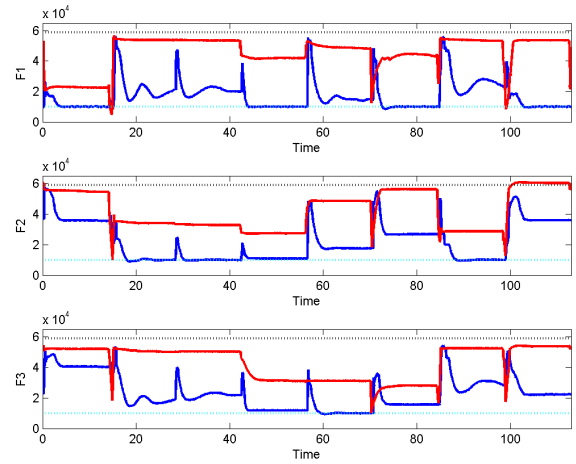


Fig. 15. Comparison of measured forces using the Jacobian based position controller of [1] (red line) and the position controller with inner force feedback (blue dashed line) for each component of tendon forces. Notice that the latter exerts higher forces only during fast transient

feedback guarantees that the system remains in well defined and controlled configurations by means of an accurate force regulation.

VI. CONCLUSIONS

In this paper we described the design of a force sensor for the control of a robotic neck actuated with tendon. The sensor has a good compromise between sensitivity and mechanical resistance. The sensor is then used for the control of the neck degrees of freedom. We show that the use of force feedback simplifies the controller and allows to deal with the intrinsic redundancy in the actuation. Moreover, by performing some experiments on the humanoid robot James, we have proved that controlling the force of the tendons is beneficial

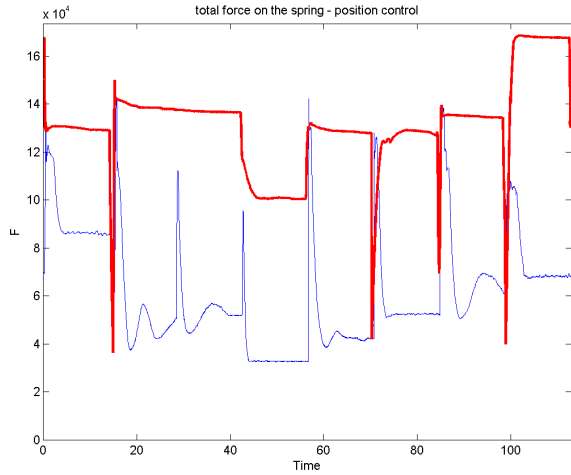


Fig. 16. Comparison of the total force acting on the spring in the two cases, using the Jacobian based position controller of [1] (red line) and using the position controller with inner force feedback (blue dashed line) for each component of tendon forces. The force control limits the total force transmitted by the tendons, thus avoiding the crush of the spring.

to reduce the stress of the structure and maintain the system in controllable configurations.

VII. ACKNOWLEDGEMENTS

The authors were supported by FP7 project CHRIS (FP7-IST-215805).

APPENDIX

A. Computing F_d given τ_d

In the proposed controller we want to solve the following optimization problem:

$$\min_{F_d \in \mathcal{F}(\tau_d)} \|F_d\| \quad s.t. \quad F_d \geq F_{min},$$

where $\mathcal{F}(\tau_d)$ is the set of all forces F_d realizing the given torques τ_d , i.e.:

$$\mathcal{F}(\tau_d) = \{F_d : \tau_d = J(\alpha, l)F_d\}.$$

This optimization problem can be reformulated as a linear-quadratic optimization problem³ which can be solved with standard optimization algorithms. In our specific case, however, we can solve the optimization analytically, exploiting the structure of the matrix J . In particular, the admissible set $\mathcal{F}(\tau_d)$ can be rewritten as:

$$\mathcal{F}(\tau_d) = \{J^\dagger \tau_d + \lambda u, \forall \lambda \in \mathbb{R}\},$$

³In general the optimization problem is not guaranteed to have a solution. However, in a system actuated with tendons in agonist-antagonist configuration, the null space of J is composed of vectors whose components are positive (i.e. vectors corresponding to a cocontraction of the tendons which only increase tendon tensions without changing the end effector forces). Practically speaking, in our case, this corresponds to the fact that shortening the cables of the same length we don't produce any movement of the head but only a increment of the tendon tensions.

where u is a generic vector in $\ker(J)$ which in our specific case has dimension one⁴. Therefore, the optimization problem can be reformulated as:

$$\min_{\lambda} \|J^\dagger \tau_d + \lambda u\|^2 \quad s.t. \quad J^\dagger \tau_d + \lambda u \geq F_{min} = \begin{bmatrix} f_{min} \\ f_{min} \\ f_{min} \end{bmatrix}.$$

where:

$$u = \begin{bmatrix} 1 \\ 1 \\ 1 \end{bmatrix} \in \ker(J). \quad (.1)$$

The solution of the optimization problem is therefore:

$$\lambda = f_{min} - \min(J^\dagger \tau_d), \quad (.2)$$

where $\min(\cdot)$ is the operator which return the smallest element in a vector.

REFERENCES

- [1] F. Nori, L. Jamone, G. Metta, and G. Sandini, "Accurate control of a human-like tendon driven neck," in *International Conference on Humanoid Robots*, Genova, Italy, 2007.
- [2] O. Holland and R. Knight, "The anthropomorphic principle," in *Symposium on Biologically Inspired Robots*, Bristol, England. AISA, April 2006.
- [3] I. Mizuuchi, T. Yoshikai, Y. Sodeyama, Y. Nakanish, A. Miyadera, T. Yamamoto, T. Niemel, M. Hayashi, J. Urata, Y. Namiki, T. Nishino, and M. Inaba, "Development of musculoskeletal humanoid kotaro," in *International Conference on Robotics and Automation (ICRA)*. IEEE, May 2006.
- [4] G. Metta, G. Sandini, D. Vernon, L. Natale, and F. Nori, "The icub humanoid robot: an open platform for research in embodied cognition," in *Workshop on Performance Metrics for Intelligent Systems*, National Institute of Standards and Technology, August 19-21 2008, Washington DC, USA.
- [5] T. Asfour, K. Regenstein, P. Azad, J. Schrder, A. Bierbaum, N. Vahrenkamp, and R. Dillmann, "ARMAR-III: An integrated humanoid platform for sensory-motor control," in *IEEE-RAS International Conference on Humanoid Robots*, December 2007, Genoa Italy.
- [6] R. Volpe and P. Khosla, "A theoretical and experimental investigation of explicit force control strategies for manipulators," *IEEE Transactions on Automation Control*, vol. 30 (11), pp. 1634–1650, November, 1993.
- [7] T. R. Kurfess, *Impedance and Interaction Control*. CRC Press, 2004, ch. 19, pp. 1–23.
- [8] L. Jamone, F. Nori, G. Metta, and G. Sandini, "James: A humanoid robot acting over an unstructured world," in *International Conference on Humanoid Robots*, Genova, Italy, 2006.
- [9] R. Verhoeven and M. Hiller, "Estimating the controllable workspace of tendon-based stewart platforms," in *7th International Symposium on Advances in Robot Kinematics (ARK)*, Portoroz, Slovenia, 2000, p. 277284.
- [10] A. Hay and J. Snyman, "Optimization of a planar tendon-driven parallel manipulator for a maximal dextrous workspace," *Engineering Optimization*, vol. 37(3), pp. 217 – 236, April 2005.
- [11] H. Clarkson, *Musculoskeletal Assessment*, 2nd ed. Lippincott Williams & Wilkins, 2000.
- [12] F. Kendall, E. McCreary, P. Provance, M. Rodgers, and W. Romani, *Muscles: Testing and Function with Posture and Pain*, 5th ed. Lippincott Williams & Wilkins, 2005.
- [13] L. Tsai, *Robot Analysis: The Mechanics of Serial and Parallel Manipulators*. Wiley-Interscience, 1999.
- [14] S. Timoshenko and J. Goodier, *Theory of Elasticity*, 3rd ed. McGraw Hill, 1970.

⁴We here use the fact that $J \in \mathbb{R}^{2 \times 3}$ is a full rank matrix.